CHEMISTRY
A EUROPEAN JOURNAL

DOI: 10.1002/chem.200903552

Seed-Mediated Synthesis of Au Nanocages and Their Electrocatalytic Activity towards Glucose Oxidation

Yue Zhang,[a, b] Fugang Xu,[a, b] Yujing Sun,[a, b] Cunlan Guo,[a, b] Kang Cui,[a, b] Yan Shi,[a, b] Zhiwei Wen,[a, b] and Zhuang Li*[a, b]

Abstract: We report a modified seed-mediated approach for the synthesis of uniform Au nanocages (AuNCs). $HAuCl_4$ was reduced in an aqueous mixture of hexamethylenetetramine (HMT), poly(*N*-vinyl-2-pyrrolidone) (PVP), and $AgNO_3$. The nanocages were (54.6 ± 13.3) nm in outer-edge length and about 12 nm in wall thickness. The structure of the AuNCs was characterized by scanning electron microscopy (SEM), transmission electron microscopy (TEM), X-ray energy dispersive spectroscopy (EDS), X-ray diffraction (XRD), Fourier-transform infrared (FTIR) spectroscopy, and X-ray photoelectron spectroscopy (XPS). Morphological changes associated with the seed-mediated growth of Au nanoparticles (AuNPs) in the absence of HMT or PVP were examined. The results demonstrate that both PVP and HMT play important roles in the formation of the nanocage structure. The function of $AgNO_3$ was also studied. A possible formation mechanism for the AuNCs was investigated by monitoring TEM images of the Au nanostructures formed at various reaction times. The electrocatalytic activity of the AuNCs towards the oxidation of glucose was explored, and a nonenzymatic glucose sensor with high sensitivity and good stability was further fabricated. To the best of our knowledge, this is the first report of the preparation of AuNCs by a seed-mediated strategy and of the application of AuNCs in the electrocatalytic oxidation of glucose. Our results should facilitate the creation of novel nanomaterials with various morphologies and the exploration of their applications in nanotechnological, optical, catalytic, and materials science fields.

Keywords: electrocatalytic oxidation · glucose · gold · nanocages · sensors

Introduction

Recently, nanostructured materials with hollow interiors have been extensively studied due to their particular optical and catalytic properties.[1] Up to now, many approaches have been developed for the synthesis of hollow nanostructures. A review from An and Hyeon categorized these methods into four classes according to how the hollow structure was formed: the Kirkendall effect, chemical etching, galvanic replacement, and the template-mediated approach.[2] By using these four approaches, hollow structures with various morphologies have been reported, such as spheres,[3] tubes,[4] necklaces,[5] rings,[6] core–shells,[1e] boxes,[7] and cages (or frames).[7b,c,8]

Among these hollow nanostructures, Au nanocages (AuNCs) or nanoframes have gained particular attention due to their unique properties. For example, AuNCs have comparable catalytic activity with Pd nanotubes in the Suzuki coupling reaction,[9] as do Pd–Au–Ag nanocages in the methyl red hydrogenation.[10] Moreover, as photocatalysts, they are more efficient than TiO_2 and ZnO in the photodegradation of azo dyes.[11] In other fields, the surface-enhanced Raman scattering (SERS) effect of Au nanoframes has also been investigated: it was observed that the aggregation of the nanoframes decreases (rather than increases) the SERS intensity,[12] which is very different behavior from that of normal SERS substrates. In addition, the reduction of the wall thickness of the Au-based nanocages would cause red-

[a] Y. Zhang, F. Xu, Y. Sun, C. Guo, K. Cui, Y. Shi, Z. Wen, Prof. Dr. Z. Li
Graduate School of the Chinese Academy of Sciences
Beijing 100039 (P.R. China)
Fax: (+86) 431-85262057
E-mail: zligroup@yahoo.com.cn

[b] Y. Zhang, F. Xu, Y. Sun, C. Guo, K. Cui, Y. Shi, Z. Wen, Prof. Dr. Z. Li
State Key Laboratory of Electroanalytical Chemistry
Changchun Institute of Applied Chemistry, Chinese Academy of Sciences
Changchun, Jilin 130022 (P.R. China)

Supporting information for this article is available on the WWW under http://dx.doi.org/10.1002/chem.200903552.

shifts in the localized surface plasmon resonance (LSPR) peak[7c] to 800–900 nm (the transparent window of soft tissues); this could lead to promising applications in the biomedical field.[13] Because of these useful properties, as well as their biocompatibility, their broad available size range (35–100 nm), their easy surface modification for targeting,[14] their absence of potential heavy metal toxicity,[15] and their strong optical absorption in the NIR region,[14b,16] much research has been carried out towards in vivo experiments using AuNCs.[17]

Much effort has been devoted to the preparation of size- and morphology-controlled AuNCs. The general synthesis method is that first reported by Xia et al., who synthesized AuNCs with uniform shape and size through a galvanic replacement reaction between Ag nanocubes and $HAuCl_4$.[18] Since then, there have been many reports of the use of this method.[1f,19] Very recently, the preparation of uniform AuNCs by using electrodeposition with Ag nanocubes as templates was reported by Torimoto et al.[8e] However, the requirement of the Ag nanocubes as sacrificial templates is a drawback in both methods.

Although there are many preparations of AuNCs, up to now, there have been no reports of the preparation of AuNCs by a seed-mediated growth approach. Herein, we report the synthesis of AuNCs using a modified four-step seed-mediated growth method. Our presented strategy is simpler than the above-described methods because it does not require the high-temperature process of fabricating Ag nanocubes. In our experiment, poly(*N*-vinyl-2-pyrrolidone) (PVP) was introduced to the reaction system as a capping agent, while hexamethylenetetramine (HMT) was used as a ligand that could coordinate to Au^{3+} to promote the formation of the nanocage structure. The introduction of $AgNO_3$ was also found to be essential for the formation of nanocages. Furthermore, a possible formation mechanism for the AuNCs was proposed based on the structure evolution at various reaction times.

The electro-oxidation of glucose has been extensively studied with a view to applications in the fields of sensors and biofuel cells. There are two reports of the use of Au nanoparticles for the enzymatic electrochemical and optical detection of glucose.[20] Nonenzymatic glucose sensors have clear advantages over enzymatic glucose sensors: their good stability, their easy immobilization, and their avoidance of the need for an expensive enzyme. In this work, we have investigated the electrocatalytic activity of the AuNCs towards the oxidation of glucose, and have tried to fabricate a nonenzymatic glucose sensor by immobilizing the AuNCs on the glassy carbon electrode (GCE). The high sensitivity and good stability of the AuNC-modified GCE (AuNC/GCE) demonstrate that the AuNC structure is potentially a good candidate for the nonenzymatic detection of glucose.

Results and Discussion

Synthesis and characterization of AuNCs: The Au seeds were synthesized according to a previously reported method[21] to give an average diameter of (4.5 ± 0.6) nm (see Figure S1 in the Supporting Information). The AuNCs were synthesized by a four-step seed growth protocol as illustrated in Figure 1. The morphology of the AuNCs obtained in vial D was then observed by using both scanning electron microscopy (SEM) and transmission electron microscopy (TEM). Figure 2A–C shows representative SEM images of the AuNCs at various magnifications. The low-magnification image (Figure 2A) indicates that the product consists of a large quantity of monodisperse square nanostructures with bright edges and dark centers. The high-magnification image (Figure 2B) indicates that the nanostructured products have hollow interiors and clear square faces resembling window panes. Further characterization of the nanostructures from a 45° view (Figure 2C) demonstrates that the nanostructures are 3D nanocages with six facets and hollow interiors. It can be observed from the TEM image (Figure 2D) that the wall thickness of the hollow nanostructure was about 12 nm. The histogram (inset of Figure 2A) shows the distribution of the outer-edge length of the nanocages ($N=100$), the average length being (54.6 ± 13.3) nm. The X-ray diffraction (XRD) pattern of the nanostructure is shown in Figure 2E. The diffraction peaks located at 38.1, 44.3, 64.7, and 77.5° can be indexed to the (111), (200), (220), and (311) planes, respectively, of the face-centered cubic (fcc) structure of gold (JCPDS No. 04-0784), which indicates that the nanostructures formed are AuNCs. The chemical composition of the AuNCs was further examined by X-ray energy dispersive spectroscopy (EDS). As shown in Figure 2F, peaks can be seen for Au, Ag, and C (the strongest peak originated from the silicon substrate), which is evidence that the AuNCs are

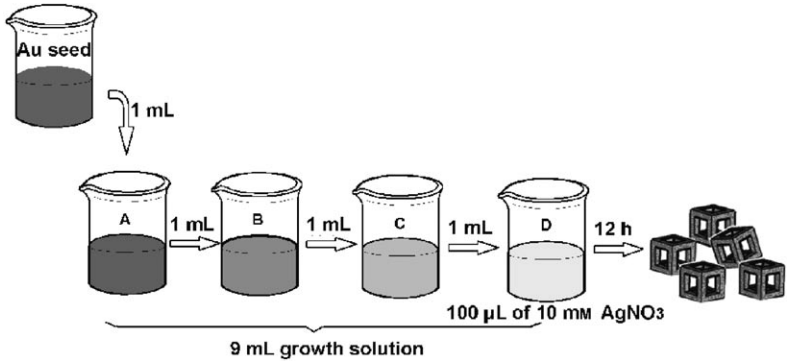

Figure 1. The general process for the fabrication of AuNCs.

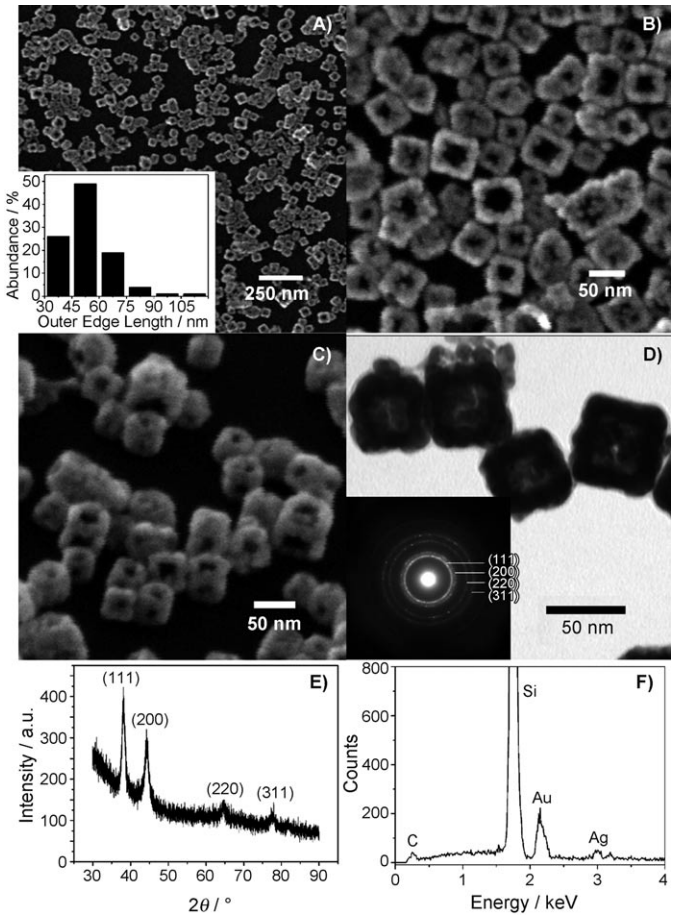

Figure 2. SEM images (A, B, C), TEM image (D), XRD pattern (E), EDS (F), and SAED (inset of D) of AuNCs. The inset image of A shows the histogram of the outer-edge length distribution of the AuNCs.

formed from $HAuCl_4$ and $AgNO_3$. The Au peak is much stronger than the Ag peak, which shows that Au is the main element comprising the nanocage structure, and this agrees well with the XRD data. The signal due to C has possibly arisen from added PVP or HMT during the synthesis. The structure of the AuNCs was further characterised by selected area electron diffraction (SAED) as shown in the inset of Figure 2D. The diffraction rings from the inside to the outside can be indexed to (111), (200), (220), and (311) of fcc gold. The SAED pattern suggests that the AuNCs have a polycrystalline structure with many smaller nanoparticles that have independent orientations.[8e]

To obtain further information about the AuNCs, Fourier-transform infrared (FTIR) spectroscopy and XPS were used to analyze the composition of the nanostructures. The band at 1649 cm^{-1} in the FTIR spectrum (Figure 3) is considered to arise from the C=O stretching mode of the PVP molecule,[22] which indicates the presence of the PVP capping agent in the AuNCs. Figure 4 shows the XPS spectra of the prepared AuNCs. In Figure 4A, the XPS spectrum of the AuNCs shows the Au $4f_{7/2}$ and $4f_{5/2}$ doublet with binding energies of 83.4 and 87.2 eV, respectively, which are the values

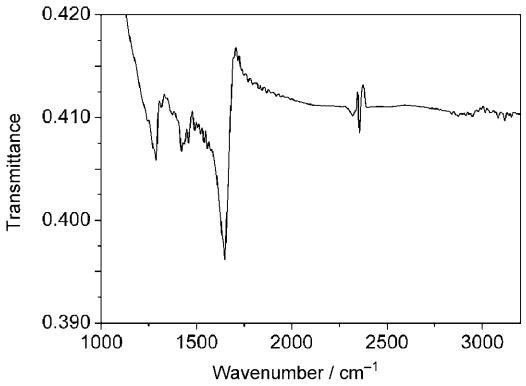

Figure 3. FTIR spectrum of AuNCs.

for Au in the zero oxidation state.[23] The two signals at 367.7 and 373.6 eV (Figure 4B) indicate the presence of metallic Ag, which is slightly shifted compared with the bulk metallic Ag due to the interaction between the Ag core and the oxygen atom in the carboxyl (C=O) of PVP.[24] The C 1s signal (Figure 4C) can be fitted to four peaks through curve fitting. The binding energies of the peaks at the positions of 284.7, 285.3, 286.1, and 287.6 eV correspond to C1–C4 in the PVP and HMT molecules.[23,24] The N 1s signal at 399.8 eV (Figure 4D) seems not to be influenced by the Au core. The FTIR and XPS data confirm the presence of both PVP and HMT molecules in the AuNCs.

Effects of PVP and HMT on controlling the shape of AuNCs: HMT has been reported to be effective in the synthesis of many structures with various morphologies, such as microtubes,[25] microrods,[26] nanorods, and nanowire arrays of ZnO,[27] Pd nanobricks,[28] branched Au nanopods,[29] and hierarchical $ZnSnO_3$ nancages.[30] PVP, on the other hand, has been used particularly frequently in the synthesis of many Au and Ag nanostructures.[23,24,31] In our work, we report the preparation of AuNCs in the presence of both HMT and PVP, which has not previously been reported. To clarify the individual functions of HMT and PVP, control experiments were performed in the absence of either HMT or PVP in the seed-mediated growth process.

When PVP was absent, the nanoparticles aggregated after the Au seeds were injected. The solution gradually turned to purple–red, and precipitation was observed after a few hours. Figure 5A shows the SEM image of the product when PVP was absent. There are only a few aggregated nanoparticles in the product. We suggest the viscidity of PVP plays an important role in the formation of cage structure. PVP macromolecules could chemically adsorb onto the surfaces of Au nanoparticles (AuNPs),[23] which would prevent aggregation of the nanocages and the further formation of larger particles. When HMT was absent, the color of solution D finally turned brick red after 12 h. Many small nanoparticles with a few large aggregated nanoparticles, hexagonal nanoparticles, and triangular nanoparticles can be seen in the final product (Figure 5B). These control experiments

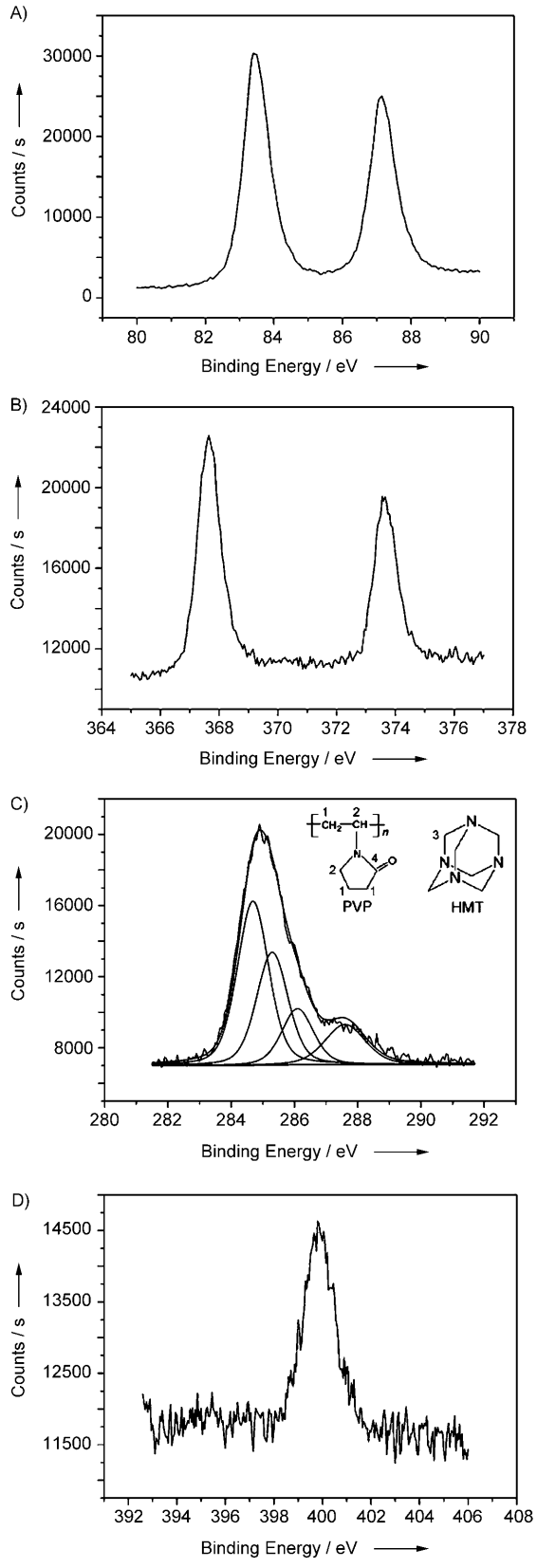

Figure 4. XPS spectra of AuNCs: Au 4f (A), Ag 3d (B), C 1s (C), and N 1s (D) regions, and the molecular structures of HMT and PVP (inset of C).

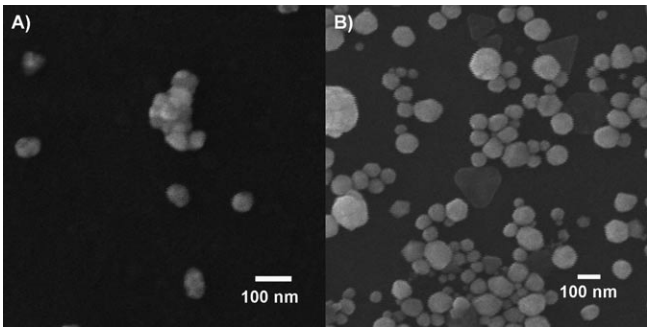

Figure 5. SEM images of the products obtained in the absence of PVP (A) and HMT (B).

indicate that both PVP and HMT play significant roles in directing the nucleation and growth of Au nanostructures. Specifically, PVP prevents the aggregation of inorganic nanoparticles, while HMT may facilitate the growth of dimensional structure to promote the formation of the nanocages.[31]

Effect of silver ions on controlling the shape of AuNCs: In vials A to C (Figure 1), without addition of $AgNO_3$, there were only small AuNPs (bigger than the seeds) formed after 12 h (data not shown here), which may be ascribed to the growth of Au seeds. Thus, $AgNO_3$ appears to play an important role in the formation of AuNCs. In a further control experiment, we investigated the function of $AgNO_3$ in the reaction system. Figure 6 shows the SEM image of AuNPs

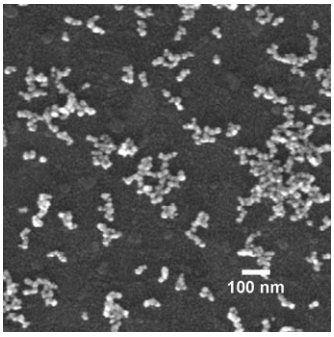

Figure 6. SEM image of the product obtained in the absence of $AgNO_3$.

synthesized in solution D in the absence of $AgNO_3$ after reaction for 12 h. It is clear that there are no nanocages, but many nanoparticles with a diameter of about 15 nm. This observation is consistent with previous reports.[21]

Furthermore, when $AgNO_3$ was replaced by HNO_3, KNO_3, or $NaNO_3$, no AuNCs were obtained (data not shown). This suggests that Ag^+ plays a vital role in the cage structure formation. The function of Ag^+ has been proposed in various synthesis systems.[21,32] It is speculated that Ag atoms are likely to be deposited preferentially on certain facets of the AuNPs by the under-potential deposition

(UPD) of silver ions,[32c] and then incorporated into the Au lattice to promote the novel Au nanostructure formation.[21]

Possible mechanism of formation of AuNCs: The morphologies of the Au nanostructures formed at different reaction times were characterized by TEM (Figure 7) to understand

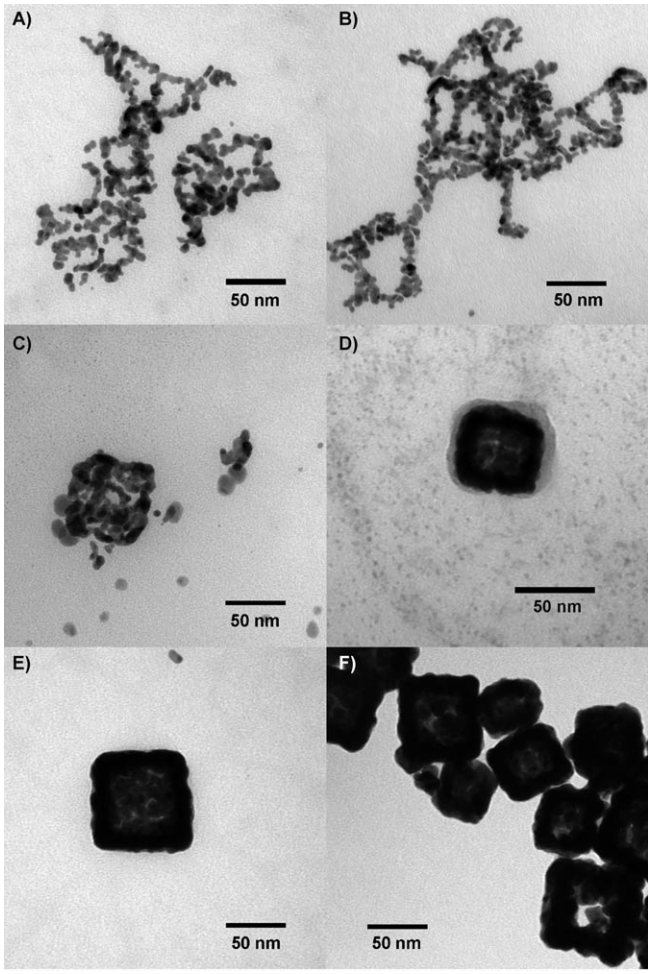

Figure 7. TEM images of the Au structures synthesized at different reaction periods with 5 min (A), 10 min (B), 20 min (C), 40 min (D), 60 min (E), and 12 h (F).

the formation mechanism of AuNCs. As shown in Figure 7A, after a short reaction time of 5 min, the AuNPs aggregated and connected to each other to form chains. The driving force for this action may be the dipole–dipole attraction between the AuNPs.[33] When the reaction was performed for 10 min (Figure 7B), the arranged chains became linked to each other and began to form an obscure cage-like structure. After 20 min of reaction, the nanoparticles fused into each other and the cage structures were clearer (Figure 7C). As the growth continued for 40 min, more nanoparticles aggregated and connected to each other through fusion of the fringes of every independent particle to form the cage-like structure (Figure 7D). After 60 min of reaction, the cage-like structure was well formed, and a square frame with hollow interior can be observed (Figure 7E). After further growth for about 12 h, the nanocages were completely synthesized. Many nanocages with outer-edge length of (54.6 ± 13.3) nm can be observed (Figure 7F).

Figure S2 in the Supporting Information shows the corresponding UV/Vis absorption spectra of solution D in the corresponding different reaction periods. No absorption band can be seen before 20 min. It is possible that Au nanostructures have formed but without a clear cage shape at this stage. After 20 min, a band at 512 nm appears, which corresponds to the formation of the Au nanostructures in Figure 7C. The position of the band then remains fixed but its intensity is stronger at 40 and 60 min. After 12 h, the position of the band redshifts to 522 nm and the intensity increases even further, which indicates the full growth of more AuNCs.

The UV/Vis spectra of the solution in vial D was monitored during the successive addition of the related reagents (Figure 8). The aqueous $HAuCl_4$ has two absorption bands

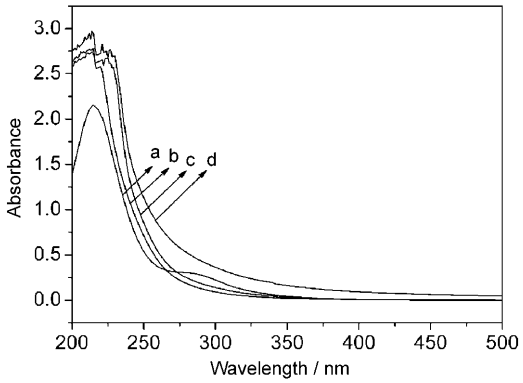

Figure 8. UV/Vis absorption spectra of the solution after addition of a) $HAuCl_4$, b) $HAuCl_4$+HMT, c) $HAuCl_4$+HMT+PVP, and d) $HAuCl_4$+HMT+PVP+$AgNO_3$.

at 215 and 287 nm (Figure 8a), corresponding to the ligand-to-metal charge-transfer band and the ligand field band of $AuCl_4^-$, respectively.[34] When HMT was added to the solution, the solution changed from yellow to clear and the two absorption bands of $HAuCl_4$ disappeared (Figure 8b). This may indicate that $HAuCl_4$ and HMT form a complex that has a dimensional structure.[35] Au^{3+} is in the third transition series with eight electrons in the outermost d shell, and it generally forms coordinative complexes with other complexants.[36] And HMT has four N atoms that have lone pair electrons. So HMT can bind to Au^{3+} and form a dimensional structure, which is very important for the formation of the cagelike structure. From Figure 8c and d, we can see that the UV/Vis absorption spectra of the solution remains unchanged after the successive addition of $AgNO_3$ and PVP, which indicates that no reaction took place after the addition of these two reagents.

Based on the above results, a possible mechanism for the formation of AuNCs is proposed, as shown in Figure 9. $HAuCl_4$ and HMT coordinate to form a complex with a cubic framelike structure. At the beginning of the reaction in vial D, the spherical Au seeds aggregate and connect to each other due to the dipole–dipole attraction of the nanoparticles. The Ag atoms deposited on the surface of the Au

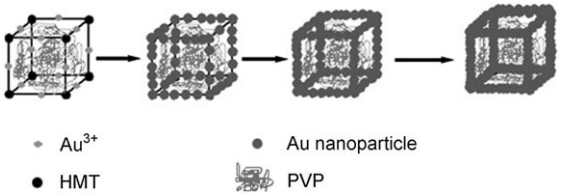

Figure 9. Schematic representation of the formation of AuNCs.

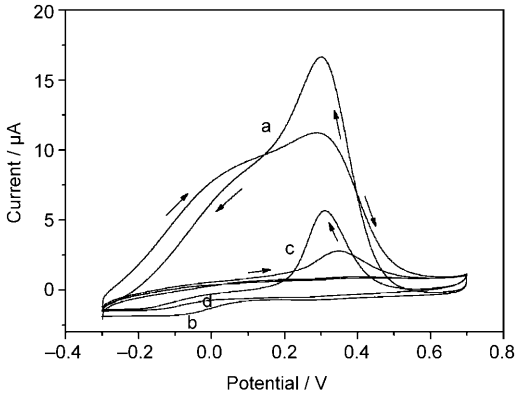

Figure 10. Cyclic voltammogram (CV) of AuNPs/GCE (a, b) and AuNCs/GCE (c, d) in 0.1 M PBS (pH 7.4) in the absence (b, d) and presence (a, c) of 50 mM glucose. Scan rate: 10 mV s^{-1}

seeds may play an assistant role in this process. Then, they self-arrange into cagelike structures along the complex formed by $HAuCl_4$ and HMT. The nanoparticles then grow bigger because of the supply of more Au in the solution. The other Au seeds dissolve and grow onto larger nanoparticles of Au cages in a process known as Ostwald ripening.[37] PVP is distributed in the interior and outside of the cage structure to prevent the aggregation of nanoparticles and support the cage framework. Finally, the nanostructures grow into cages by stacking faults and by the fusion of the fringes of every independent particle. However, the details for the formation mechanism of AuNCs are still not very clear, and more work is required to confirm our hypothesis.

Electrocatalytic oxidation of glucose: The AuNCs synthesized in our experiment have a high surface-to-volume ratio, which inspired us to investigate their electrocatalytic activity towards glucose oxidation. This was done by modifying a GCE with AuNCs. AuNPs with a diameter of (56.3 ± 3.1) nm were also used to modify a GCE (AuNP/GCE) for comparison. Figure 10 shows the cyclic voltammogram (CV) of the oxidation of glucose at AuNC/GCE and AuNP/GCE in PBS (pH 7.4) containing 50 mM glucose at a scan rate of 10 mV s^{-1}. No current response to glucose was observed in the absence of glucose (see curves b and d). After glucose was injected, AuNC/GCE (Figure 10, curve a) showed a higher current response than AuNP/GCE (curve c), which we ascribe to the larger electrochemically active area of the AuNCs. The CV of AuNC/GCE in the positive potential scan shows two anodic current peaks located at 0.04 and 0.29 V. The reaction kinetics of glucose electro-oxidation were sensitive to the crystallographic orientation of the electrode surface.[38] The electrochemical oxidation of glucose on the surface of polycrystalline gold in PBS has been reported to give rise to two peaks in both the positive and negative potential scans.[38b] The formation of an $(OH)_{ads}$ layer on the gold surface is the first step for the electro-oxidation of glucose. The oxidation of glucose is reported to be through the interaction between the hemiacetal group and $(OH)_{ads}$. The hydrogen bound to carbon atom C1 is the first to be oxidized on the AuNC, and an adsorbed intermediate is formed. The first peak at 0.04 V can be attributed to this electrochemical process. One proton from each glucose is released in this step.[38] As the potential becomes more positive, the adsorbed intermediate is further oxidized to form gluconolactone, resulting in the direct oxidation of glucose at 0.29 V.[38] Another proton is released in this step. Then, gluconolactone is desorbed from the electrode and hydrolyzed to form sodium gluconate in PBS. The whole process involves the transfer of two electrons per glucose molecule. After the potential of 0.29 V, gold oxide forms on the surface and occupies the active sites of the electrode, which inhibits the oxidation of glucose and lead to a decrease in current. In the negative potential scan process, the surface gold oxide is reduced and enough surface active sites can be obtained for the direct oxidation of glucose, leading to an anodic current peak at 0.30 V. As the potential moves to more negative values, an anodic current peak at 0.04 V corresponding to the first peak in the positive potential appears. These results are in agreement with previous reports.[39] It is noticeable that the electro-oxidation of glucose occurs in a neutral solution without the need for a basic solution, indicating the excellent catalytic performance of the AuNCs.

The performance of AuNC/GCE towards glucose oxidation has been tested by recording the amperometric response (Figure 11). Considering that ascorbic acid (AA) and uric acid (UA) have interfering effects in the detection of glucose at relatively positive potentials, we investigated the optimal potential for the selective detection of glucose. The potential of 0 V was chosen for the detection. Under this optimal potential, glucose was successively injected into the PBS solution. The corresponding calibration curve is shown in the inset of Figure 11. The amperometric response to glucose shows a linear range from 0.2 to 13.4 mM ($R = 0.997$). Compared with previous reports, this is a promising sensor that could be used in the detection of glucose at low concentration.[39] The upper limit of the linear relationship is

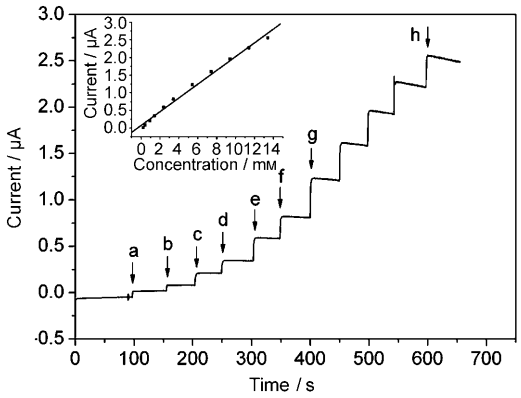

Figure 11. Amperometric response of the sensor for glucose at AuNC/GCE at 0 V. Glucose was injected successively into the stirred 0.1 M PBS (pH 7.4) with a→b 0.2 mM, c→d 0.5 mM, e→f 1 mM, g→h 2 mM. (Inset: Calibration curve of the glucose sensor.)

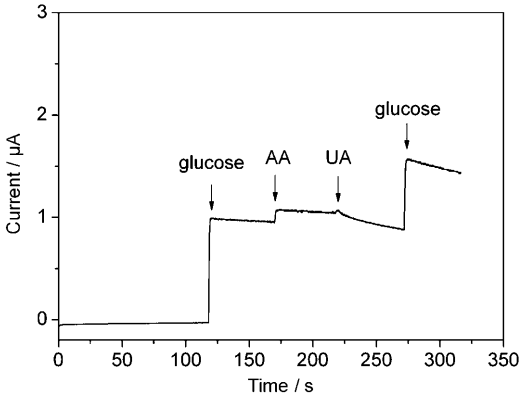

Figure 12. Current responses of AuNC/GCE to the sequential additions of 3 mM glucose, 0.1 mM AA, 0.01 mM UA, and 3 mM glucose at 0 V.

13.4 mM, which is higher than the normal physiological level (3–8 mM), while the limit of detection is down to 5 μM with a signal to noise ratio of 3. Moreover, this nonenzymatic glucose sensor does not need additional supports, such as carbon nanotubes or graphene. Table 1 shows the analytical parameters for glucose sensors obtained with state-of-the-art noble-metal nanostructures and carbon-supported metal nanomaterials. The detection limit of this glucose sensor on AuNC/GCE is lower than or comparable with the supported-metal nanomaterials, and the detection range on AuNC/GCE is also broader.

Figure 12 shows the selectivity of AuNC/GCE under the potential of 0 V in the presence of 0.1 mM AA and 0.01 mM UA. It is clear that AA and UA interfered very little with the detection of glucose at physiological levels. After the injection of AA and UA, the AuNC/GCE retains 70% of its original current response to glucose, which suggests an improved anti-interference capability. Moreover, AuNC/GCE can be cleaned simply in 0.1 M H_2SO_4 before each measurement. After one month, the peak potential for the oxidation of glucose shows no change and the peak current decreases only a little, indicating that AuNC/GCE is stable over this period and can be used repeatedly. The results demonstrate that the AuNC-modified electrode is a promising candidate for the fabrication of nonenzymatic glucose sensors.

Table 1. Analytical parameters obtained with various glucose sensors.

Electrode	Detection potential [V]	Detection limit [μM]	Linear range [mM]	Sensitivity [$\mu A\,cm^{-2}\,mM^{-1}$]	Ref.
macroporous Au	0.35	5	2–10	11.8	[40]
PtNP-deposited MWCNTs[a]	0.7	3	1–7	591.33	[41]
Pt nanotubes	0.4	1	2–14	0.1	[42]
Au nanoparticles	0.7	below 500	0.5–8	160	[43]
Nafion/OMCs[b]	0.35	156.52	0.5–15	0.053	[44]
graphene–GOD[c]–PFIL[d]	−0.5	–	2–14	–	[45]
Gox[e]-xGnP[f]-Nafion	–	10	up to 6	11.17	[46]
mesoporous platinum	0.4	–	0–10	9.6	[47]
AuNCs	0	5	0.2–13.4	2.79	this work

[a] Multiwalled carbon nanotubes. [b] Ordered mesoporous carbon atoms. [c], [e] Glucose oxidase. [d] Polyethylenimine-functionalized ionic liquid nanocomposites. [e] Exfoliated graphite nanoplatelets.

Conclusion

For the first time, a modified seed-mediated growth approach is reported for the fabrication of uniform AuNCs without the use of solid templates. The functions of the reagents were investigated in detail. After monitoring the time-dependent morphology changes in the Au nanostructures, a possible mechanism for the growth of the nanocages could be proposed. Moreover, due to the large surface-to-volume ratio, the AuNCs exhibit good electrocatalytic properties towards the oxidation of glucose, which may find potential applications in catalytic devices and electrochemical sensors. Our work here may open up new ways for the fabrication of other novel structures and for the application of the optical and catalytic properties of the materials.

Experimental Section

Materials: $HAuCl_4{\cdot}4H_2O$, $C_6H_{12}N_4$, and $AgNO_3$ were purchased from Shanghai Chemical Reagent Co. (Shanghai, China). $C_6H_5Na_3O_7{\cdot}2H_2O$, $NaBH_4$, AA $C_6H_8O_6$, PVP (K30), and phosphate ($NaH_2PO_4{\cdot}2H_2O$ and $Na_2HPO_4{\cdot}12H_2O$) were purchased from Beijing Chemical Co. (Beijing, China). β-D-glucose was purchased from Shanghai Sinopharm Chemical Reagent Co. (Shanghai, China). 2-Mercaptosuccinic acid (MSA) and UA were purchased from Sigma–Aldrich. All of these chemicals and materials were analytical grade and were used as received without further purification. All glassware and stirrer bars were cleaned with aqua regia solution and then rinsed thoroughly with water before use. Ultrapure water (18.2 MΩ cm) produced by a Milli-Q system was used as the solvent throughout this work.

Preparation of Au seeds: The seeds were synthesized according to a previously reported method.[20] In brief, an aqueous solution (20 mL) of $HAuCl_4$ (2.5×10^{-4} M) and trisodium citrate (2.5×10^{-4} M) was first prepared. Then, ice-cold 0.01 M $NaBH_4$ (0.6 mL dissolved in 2.5×10^{-4} M trisodium citrate) was added to the prepared solution under rapid stirring. The color of the solution immediately turned to orange–red, which indicated the formation of the AuNPs. The seed solution was maintained at room temperature for about 2 h before use.

Synthesis of AuNCs: The AuNCs were prepared by a four-step seed-mediated growth protocol as illustrated in Figure 1. First, four vials labeled A–D were prepared. Growth solution (9 mL) containing 2.5×10^{-4} M $HAuCl_4$, 0.1 M HMT, and 0.1 M PVP was added to each vial. An extra 100 μL of 0.01 M $AgNO_3$ was added only to vial D. Then, 0.08 M ascorbic acid (50 μL) was added to each vial. Next, the seed solution (1.0 mL) was mixed with the solution in vial A. After stirring for a few seconds, 1.0 mL of the solution in vial A was transferred to vial B. The same transfer was repeated twice (from vial B to C and C to D). The color of solution D changed from clear to slightly gray–blue after about 20 min and then to purple–blue after 60 min. On standing, the color of the solution became a little darker. After 12 h, the solution in vial D was used for further characterization.

The control experiments were performed as follows: all other conditions were the same, except HMT or PVP was absent.

Synthesis of (56.3±3.1) nm AuNPs: AuNPs were also synthesized by a seed-mediated method according to the literature[48] with a little modification. First, Au seeds with a diameter of (15.0±1.2) nm were prepared by the citrate-reduction procedure of Frens.[49] Then, these Au seeds (1.056 mL) were mixed with 12 mM $HAuCl_4$ (835 μL) and water (38 mL). After that, 0.01 M MSA (600 μL) was injected into the solution with vigorous stirring. The reaction was complete after 1 h. Finally, AuNPs with a diameter of (56.3±3.1) nm were obtained (Figure S3 in the Supporting Information).

Preparation of AuNC/GCE and AuNP/GCE: After the preparation of the AuNCs, 3 mL of the solution in vial D was transferred to an empty tube and water (3 mL) was added. The solution was centrifuged at 12000 rpm for 10 min, and then thoroughly rinsed with ethanol (6 mL) and water (6 mL). Finally, the sample was dispersed in ultrapure water (50 μL). After ultrasonic treatment, 10 μL of the sample was added dropwise onto the GCE that had been carefully polished with alumina slurry (1.0, 0.3, and 0.05 μm, successively) and dried in the air. Then, Nafion (0.5%, 5 μL) was added dropwise onto the surface of the electrode and left to dry.

The AuNPs of (56.3±3.1) nm were centrifuged and a solution of AuNPs was obtained. The solutions of AuNCs and AuNPs were characterized by inductively coupled plasma mass spectroscopy (ICP-MS). After that, a certain amount of AuNPs was dropped onto the GCE, ensuring that the contents of Au on both modified electrodes were the same. After the electrode was dried, Nafion (0.5%, 5 μL) was added dropwise onto the surface of the electrode.

Instrumentation: UV/Vis spectra were obtained by using a UV/Vis spectrophotometer (UV mini1240, Shimadzu Instruments, Japan) at room temperature. SEM, and EDS measurements were carried out on an XL30 ESEM FEG scanning electron microscope equipped with an energy dispersive X-ray analyzer at an accelerating voltage of 20 kV. TEM and SAED analyses were carried out by using a JEOL JEM-1011 transmission electron microscope with an accelerating voltage of 100 kV. For TEM measurements, a drop of the sample was prepared by placing a certain amount of the solution on a carbon-coated copper grid and dried at room temperature. FTIR measurements were conducted on a BRUKER Vertex 70 FTIR spectrometer operated at 4 cm^{-1} resolution. XPS was performed by using an ESCALAB-MKII spectrometer (VG Co., United Kingdom) with $Al_{K\alpha}$ X-ray radiation as the source for excitation. Atomic force microscope (AFM) images (see Supporting Information) were obtained with a Digital Instruments Nanoscope IIIa (Santa Barbara, CA) in tapping mode in air under ambient conditions. XRD patterns were recorded with a Rigaku-D/max 2500 V X-ray diffractometer equipped with a $Cu_{K\alpha}$ radiation source ($\lambda=1.54178$ Å). The content of Au was determined by using ICP-MS (X Series 2 Thermo Scientific, USA). All electrochemical experiments were performed by using a CHI-800 electrochemical workstation (Shanghai, China) in a conventional three-electrode cell containing PBS (0.1 M, pH 7.4) at room temperature, using a platinum wire as the auxiliary electrode, an Ag/AgCl (saturated KCl) electrode as the reference electrode, and AuNC/GCE (3.0 mm in diameter) as the working electrode. Before each electrochemical experiment, N_2 was used to deaerate the solution for 10 min in to exclude interference from O_2.

Acknowledgements

This work was supported by the National Natural Science Foundation of China (20775077) and the Chinese Academy of Sciences (KJCX2-YW-H11). Financial support by the National Basic Research Program of China (973 Program; no. 2010CB933600) is gratefully acknowledged.

[1] a) Y. Li, T. Kunitake, S. Fujikawa, *J. Phys. Chem. B* **2006**, *110*, 13000; b) Y. H. Ng, S. Ikeda, T. Harada, S. Higashida, T. Sakata, H. Mori, M. Matsumura, *Adv. Mater.* **2007**, *19*, 597; c) Y. D. Yin, R. M. Rioux, C. K. Erdonmez, S. Hughes, G. A. Somorjai, A. P. Alivisatos, *Science* **2004**, *304*, 711; d) F. B. Su, F. Y. Lee, L. Lv, J. J. Liu, X. N. Tiax, X. S. Zhao, *Adv. Funct. Mater.* **2007**, *17*, 1926; e) S. Zhou, B. Varughese, B. Eichhorn, G. Jackson, K. Mcllwrath, *Angew. Chem.* **2005**, *117*, 4615; *Angew. Chem. Int. Ed.* **2005**, *44*, 4539; f) J. Chen, B. Wiley, Z. Li, D. Campbell, F. Saeki, H. Cang, L. Au, J. Lee, X. Li, Y. Xia, *Adv. Mater.* **2005**, *17*, 2255; g) J. Lee, J. C. Park, H. Song, *Adv. Mater.* **2008**, *20*, 1523.

[2] K. An, T. Hyeon, *Nano Today* **2009**, *4*, 359.

[3] a) S. Peng, S. Sun, *Angew. Chem.* **2007**, *119*, 4233; *Angew. Chem. Int. Ed.* **2007**, *46*, 4155; b) A. Cabot, R. K. Smith, Y. Yin, H. Zheng, B. M. Reinhard, H. Liu, A. P. Alivisatos, *ACS Nano* **2008**, *2*, 1452; c) Y. Wang, L. Cai, Y. Xia, *Adv. Mater.* **2005**, *17*, 473; d) H. P. Liang, L. J. Wan, C. L. Bai, L. Jiang, *J. Phys. Chem. B* **2005**, *109*, 7795; e) H. P. Liang, H. M. Zhang, J. S. Hu, Y. G. Guo, L. J. Wan, C. L. Bai, *Angew. Chem.* **2004**, *116*, 1566; *Angew. Chem. Int. Ed.* **2004**, *43*, 1540; f) M. Chen, L. Gao, *Inorg. Chem.* **2006**, *45*, 5145; g) S. Guo, Y. Fang, S. Dong, E. Wang, *J. Phys. Chem. C* **2007**, *111*, 17104; h) Y. Vasquez, A. K. Sra, R. E. Schaak, *J. Am. Chem. Soc.* **2005**, *127*, 12504; i) S. Guo, S. Dong, E. Wang, *Chem. Eur. J.* **2008**, *14*, 4685.

[4] a) Y. Sun, Y. Xia, *J. Am. Chem. Soc.* **2004**, *126*, 3892; b) Y. Sun, B. J. Wiley, Z. Y. Li, Y. Xia, *J. Am. Chem. Soc.* **2004**, *126*, 9399; c) Y. Sun, Y. Xia, *Adv. Mater.* **2004**, *16*, 264.

[5] a) J. Gao, B. Zhang, X. Zhang, B. Xu, *Angew. Chem.* **2006**, *118*, 1242; *Angew. Chem. Int. Ed.* **2006**, *45*, 1220; b) H. P. Liang, Y. G. Guo, H. M. Zhang, J. S. Hu, L. J. Wan, C. L. Bai, *Chem. Commun.* **2004**, 1496; c) J. Zeng, J. Huang, W. Lu, X. Wang, B. Wang, S. Zhang, J. Hou, *Adv. Mater.* **2007**, *19*, 2172.

[6] Y. Sun, Y. Xia, *Adv. Mater.* **2003**, *15*, 695.

[7] a) K. An, S. G. Kwon, M. Park, H. B. Na, S. I. Baik, J. H. Yu, D. Kim, J. S. Son, Y. W. Kim, I. N. Song, W. K. Moon, H. M. Park, T. Hyeon, *Nano Lett.* **2008**, *8*, 4252; b) Y. Xiong, B. Wiley, J. Chen, Z. Y. Li, Y. Yin, Y. Xia, *Angew. Chem.* **2005**, *117*, 8127; *Angew. Chem. Int. Ed.* **2005**, *44*, 7913; c) X. Lu, L. Au, J. McLellan, Z. Y. Li, M. Marquez, Y. Xia, *Nano Lett.* **2007**, *7*, 1764.

[8] a) S. Skrabalak, J. Chen, Y. Sun, X. Lu, L. Au, C. M. Cobley, Y. Xia, *Acc. Chem. Res.* **2008**, *41*, 1587; b) C. H. Kuo, M. H. Huang, *J. Am. Chem. Soc.* **2008**, *130*, 12815; c) D. Kim, J. Park, K. An, N. K. Yang, J. G. Park, T. Hyeon, *J. Am. Chem. Soc.* **2007**, *129*, 5812; d) K. Okazaki, J. Yasuia, T. Torimoto, *Chem. Commun.* **2009**, 2917; e) X. Wang, H. Fu, A. Peng, T. Zhai, Y. Ma, F. Yuan, J. Yao, *Adv. Mater.* **2009**, *21*, 1636.

[9] Y. Sun, B. Mayers, Y. Xia, *Adv. Mater.* **2003**, *15*, 641.

[10] C. M. Cobley, D. J. Campbell, Y. Xia, *Adv. Mater.* **2008**, *20*, 748.

[11] C. W. Yen, M. A. Mahmoud, M. A. El-Sayed, *J. Phys. Chem. A* **2009**, *113*, 4340.

[12] M. A. Mahmoud, M. A. El-Sayed, *Nano Lett.* **2009**, *9*, 3025.

[13] N. G. Portney, M. Ozkan, *Anal. Bioanal. Chem.* **2006**, *384*, 620.
[14] a) S. E. Skrabalak, J. Chen, L. Au, X. Lu, X. Li, Y. Xia, *Adv. Mater.* **2007**, *19*, 3177; b) J. Chen, F. Saeki, B. J. Wiley, H. Cang, M. J. Cobb, Z. Y. Li, L. Au, H. Zhang, M. B. Kimmey, X. Li, Y. Xia, *Nano Lett.* **2005**, *5*, 473.
[15] A. G. Cuenca, H. Jiang, S. N. Hochwald, M. Delano, W. G. Cance, S. R. Grobmyer, *Cancer* **2006**, *107*, 459.
[16] M. Hu, J. Y. Chen, Z. Y. Li, L. Au, G. V. Hartland, X. D. Li, M. Marquez, Y. Xia, *Chem. Soc. Rev.* **2006**, *35*, 1084.
[17] a) X. Yang, S. E. Skrabalak, Z. Y. Li, Y. Xia, L. V. Wang, *Nano Lett.* **2007**, *7*, 3798; b) K. H. Song, C. Kim, C. M. Cobley, Y. Xia, L. V. Wang, *Nano Lett.* **2009**, *9*, 183.
[18] Y. Sun, Y. Xia, *Science* **2002**, *298*, 2176.
[19] a) J. Chen, J. M. Mclellan, A. Siekkinen, Y. Xiong, Z. Y. Li, Y. Xia, *J. Am. Chem. Soc.* **2006**, *128*, 14776; b) L. Au, X. Lu, Y. Xia, *Adv. Mater.* **2008**, *20*, 2517.
[20] a) M. Zayats, E. Katz, R. Baron, I. Willner, *J. Am. Chem. Soc.* **2005**, *127*, 12400; b) M. Zayats, R. Baron, I. Popov, I. Willner, *Nano Lett.* **2005**, *5*, 21.
[21] H. L. Wu, C. H. Chen, M. H. Huang, *Chem. Mater.* **2009**, *21*, 110.
[22] a) Y. Yang, W. Wang, J. Li, J. Mu, H. Rong, *J. Phys. Chem. B* **2006**, *110*, 16867; b) C. I. Yoo, D. Seo, B. H. Chung, I. S. Chung, H. Song, *Chem. Mater.* **2009**, *21*, 939; c) K. Chan, L. E. Kostun, W. E. Tenhaeff, K. K. Gleason, *Polymer* **2006**, *47*, 6941.
[23] P. Jiang, J. J. Zhou, R. Li, Z. L. Wang, S. S. Xie, *Nanotechnology* **2006**, *17*, 3533.
[24] a) H. H. Huang, X. P. Ni, G. L. Loy, C. H. Chew, K. L. Tan, F. C. Loh, J. F. Deng, G. Q. Xu, *Langmuir* **1996**, *12*, 909; b) P. Jiang, S. Y. Li, S. S. Xie, Y. Gao, L. Song, *Chem. Eur. J.* **2004**, *10*, 4817.
[25] L. Vayssieres, K. Keis, A. Hagfeldt, S. E. Lindquist, *Chem. Mater.* **2001**, *13*, 4395.
[26] L. Vayssieres, K. Keis, S. E. Lindquist, A. Hagfeldt, *J. Phys. Chem. B* **2001**, *105*, 3350.
[27] L. Vayssieres, *Adv. Mater.* **2003**, *15*, 464.
[28] A. A. Umar, M. Oyama, *Cryst. Growth Des.* **2008**, *8*, 1808.
[29] A. Ali Umar, M. Oyama, *Cryst. Growth Des.* **2009**, *9*, 1146.
[30] Y. Zeng, T. Zhang, H. Fan, W. Fu, G. Lu, Y. Sui, H. Yang, *J. Phys. Chem. C* **2009**, *113*, 19000.
[31] a) B. Wiley, Y. Sun, B. Mayers, Y. Xia, *Chem. Eur. J.* **2005**, *11*, 454; b) J. Han, Y. Liu, R. Guo, *Adv. Funct. Mater.* **2009**, *19*, 1112; c) S. Guo, D. Wen, S. Dong, E. Wang, *Talanta* **2009**, *77*, 1510.
[32] a) H. M. Chen, R. S. Liu, D. P. Tsai, *Cryst. Growth Des.* **2009**, *9*, 2079; b) M. Liu, P. Guyot-Sionnest, *J. Phys. Chem. B* **2005**, *109*, 22192; c) D. Seo, C. I. Yoo, J. C. Park, S. M. Park, S. Ryu, H. Song, *Angew. Chem.* **2008**, *120*, 775; *Angew. Chem. Int. Ed.* **2008**, *47*, 763.
[33] Z. Tang, N. A. Kotov, M. Giersig, *Science* **2002**, *297*, 237.
[34] K. Torigoe, K. Esumi, *Langmuir* **1992**, *8*, 59.
[35] N. Katsaros, J. M. Tsangaris, G. M. Tsangaris, *Monatsh. Chem.* **1983**, *114*, 27.
[36] A. K. Gangopadhayay, A. Chakravorty, *J. Chem. Phys.* **1961**, *35*, 2206.
[37] A. R. Roosen, W. C. Carter, *Physica* **1998**, *261*, 232.
[38] a) S. Cho, H. Shin, C. Kang, *Electrochim. Acta* **2006**, *51*, 3781; b) M. W. Hsiao, R. R. Adzic, E. B. Yeager, *J. Electrochem. Soc.* **1996**, *143*, 759.
[39] a) Y. P. Sun, H. Buck, T. E. Mallouk, *Anal. Chem.* **2001**, *73*, 1599; b) W. Zhao, J. J. Xu, C. G. Shi, H. Y. Chen, *Electrochem. Commun.* **2006**, *8*, 773; c) H. Zhang, J. J. Xu, H. Y. Chen, *J. Phys. Chem. C* **2008**, *112*, 13886.
[40] Y. Li, Y. Y. Song, C. Yang, X. H. Xia, *Electrochem. Commun.* **2007**, *9*, 981.
[41] D. Wen, X. Zou, Y. Liu, L. Shang, S. Dong, *Talanta* **2009**, *79*, 1233.
[42] J. K. Yuan, K. Wang, X. H. Xia, *Adv. Funct. Mater.* **2005**, *15*, 803.
[43] F. Kurniawan, V. Tsakova, V. M. Mirsky, *Electroanalysis* **2006**, *18*, 1937.
[44] M. Zhou, L. Shang, B. Li, L. Huang, S. Dong, *Biosens. Bioelectron.* **2008**, *24*, 442.
[45] C. S. Shan, H. F. Yang, J. F. Song, D. X. Han, A. Ivaska, L. Niu, *Anal. Chem.* **2009**, *81*, 2378.
[46] J. Lu, L. T. Drzal, R. M. Worden, I. Lee, *Chem. Mater.* **2007**, *19*, 6240.
[47] S. Park, T. D. Chung, H. C. Kim, *Anal. Chem.* **2003**, *75*, 3046.
[48] J. Niu, T. Zhu, Z. Liu, *Nanotechnology* **2007**, *18*, 325607.
[49] G. Frens, *Nature* **1973**, *241*, 20.

Received: December 26, 2009
Published online: June 25, 2010

